

Numerical simulation of the fluid flow through valves based on Large Eddy Simulation models

J Rigola¹, O Lehmkuhl², A Oliva¹, C D Pérez-Segarra¹

¹ Centre Tecnològic de Transferència de Calor (CTTC)
Universitat Politècnica de Catalunya (UPC), Spain

² Termo Fluids, SL, Spain

The aim of this paper is to carry out a group of numerical experiments over the fluid flow through the valve reed, using the CFD&HT code TermoFluids, a new unstructured and parallel object-oriented CFD code for accurate and reliable solving of industrial flows (1). In all studied cases a multi-dimensional explicit finite volume fractional-step based algorithm has been used with symmetry preserving discretization scheme. When turbulence modelling is needed, an extension of the Yoshizawa non-equilibrium fixed-parameter subgrid-scale (2) model to non-structured meshes is used. The pressure equation is solved by means of parallel Fourier Schur decomposition solver which is an efficient direct solver for loosely coupled PC clusters (3).

In fact, the fluid flow is analysed by two parallel phenomena (an entrance flow through a channel and a free jet through a surface). In that sense, the present paper is focused on the numerical simulation model of the fluid flow through the valve reeds, considering a simplified geometry of an axial hole plus a radial diffuser.

The numerical results presented are based on a specific geometry – orifice diameter d is 3 times valve reed diameter D -together with a wide range of boundary conditions: different Reynolds number at the entrance and different valve displacement s vs. orifice diameter d . The studied cases vary from laminar to turbulent flow, almost to be considered incompressible and lower supersonic conditions and/or choked flow.

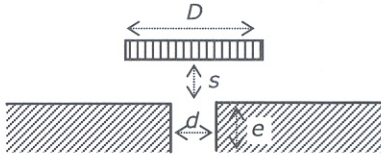
NOMENCLATURE

A_F	Effective force area (m)	p	pressure (Pa)
C	Convective operator	p_d	downstream pressure (Pa)
d	Orifice diameter (m)	p_u	upstream pressure (Pa)
D	Valve reed diameter (m)	s	gap distance (m)
D	Diffusive operator	τ	stress tensor
e	Valve plate thickness (m)	u	velocity vector (ms ⁻¹)
G	Gradient operator	Y	Compressibility factor
$(KA)_e$	Effective flow area (m ²)	Δt	time step (s)
L	Laplacian operator	ρ	fluid density (kgm ⁻³)
M	Divergence operator	ν	viscosity (Pas)

1 INTRODUCTION

One of the most important aspects of compressor design and efficiency improvements is to fully understand the fluid flow phenomena through compressor valve and consequently the parameters which define its behaviour

The methodology proposed by (4) is based on two parameters: i) effective flow area $(KA)_e$ that relates the actual mass flow rate with an ideal mass flow rate per unit flow area (assuming isentropic contraction process) defined in equation (1); and ii) the effective force area A_F defined as ratio of the actual net force on the valve and the force obtained assuming a constant pressure drop distribution, defined in equation (2), the most usual method for valve analysis and compressor design (5).



$$\dot{m} = (KA)_e (\rho v)_{id} = (KA)_e Y \sqrt{2\rho_u (p_u - p_d)} \quad (1)$$

$$F = (p_u - p_d) A_F \quad (2)$$

Figure 1. Cross sectional valve diagram.

One of the first semi-analytical models for predicting these coefficients were developed by (6) and (7). More accurate predictions need obviously the use of the multidimensional simulation of the flow through the valve like (8) which analyzed in detail the laminar flow through these valves comparing numerical and experimental results. Later, (9) studied the turbulent flow in reed type valves using the well known RNG k- ϵ model. In the same way, and based on the same low Reynolds number two-equation k- ϵ turbulence models for general purposes (10) a numerical study of the turbulent fluid-flow through valves (11) was also carried out.

The present paper represents a new advance over the numerical results over Large Eddy Simulation models presented in (12) assuming angular symmetry across cylindrical domain instead of previous plane periodical conditions.

The numerical results presented are based on a specific geometry with a valve diameter vs. orifice diameter ratio $d/D = 3$, with a wide range of boundary conditions: Reynolds number from 600 to 6000 and valve displacement vs. valve diameter s/d from 0.1 to 0.9. The final objective of these series of numerical studies are going to be a detailed parametrization of the mean valve parameters $(KA)_e$ and A_F , together with a general numerical correlation as a function of its different conditions.

2 CFD&HT CODE (TERMOFLUIDS)

The radial outflow between two coaxial disks is technologically important for different applications where valve reeds are one of them. In these cases the flow is quite complex, the pressure gradient may be either positive or negative depending on radial location. The velocity is coupled with pressure field and the conditions under which the flow will be turbulent or laminar are not clearly established. Thus, turbulence models are critical on the numerical resolution, while the numerical results expected using the parallel, unstructured and object oriented code TermoFluids described below are going to clarify it.

Some papers from the scientific literature are focused on this problem, experimentally (13)(14) under similar studied ranges allowing validate the numerical results obtained, or numerically (15)(16) based in Direct Numerical Simulations although far from the studied ranges. The numerical results presented now are a first step to a complete study of a wide range of Re numbers and disk geometries, with the final objective to describe the fluid flow phenomena and the forces generated through compressor valves.

A general view of the most important details about Navier-Stokes equation discretization and Large Eddy Simulation model used are here presented.

2.1 Discrete Navier-Stokes equations

The Navier-Stokes and continuity equations can be written as

$$\rho \frac{\partial \mathbf{u}}{\partial t} + \mathbf{C}(\mathbf{u})\mathbf{u} + \mathbf{D}\mathbf{u} + \mathbf{G}\mathbf{p} = 0 \quad (3)$$

$$\mathbf{M}\mathbf{u} = 0 \quad (4)$$

where $\mathbf{u} \in \mathbb{R}^m$ and $\mathbf{p} \in \mathbb{R}^q$ are the velocity vector and pressure, respectively. The matrices $\mathbf{C}(\mathbf{u})$, $\mathbf{D} \in \mathbb{R}^{m \times m}$ are the convective and diffusive operators, respectively. Note the \mathbf{u} -dependence of the convective operator (non-linear operator). Finally, $\mathbf{G} \in \mathbb{R}^{m \times q}$ represents the gradient operator, and the matrix $\mathbf{M} \in \mathbb{R}^{q \times m}$ is the divergence operator.

For the temporal discretization of the momentum equation (3), a second order backward difference scheme for the time derivative term, a fully explicit second-order one-leg scheme (17) for the right-hand-side terms of the momentum equation except the pressure gradient ($\mathbf{R}(\mathbf{u}_c) \doteq \Omega^{-1} - \mathbf{C}(\mathbf{u}_c)\mathbf{u}_c - \mathbf{D}(\mathbf{u}_c)$), and a first-order backward Euler scheme for the pressure gradient are used. Incompressibility constraint is treated implicit,

$$\mathbf{M}\mathbf{u}_c^{n+1} = 0 \quad (5)$$

$$\frac{(\beta + 1/2)\mathbf{u}_c^{n+1} - 2\beta\mathbf{u}_c^n + (\beta - 1/2)\mathbf{u}_c^{n-1}}{\Delta t} = \mathbf{R}((1 + \beta)\mathbf{u}_c^n - \beta\mathbf{u}_c^{n-1}) - \mathbf{G}_c\mathbf{p}_c^{n+1} \quad (6)$$

where the parameter β is computed each time-step to adapt the linear stability domain of the time-integration scheme to the instantaneous flow conditions in order to use the maximum Δt possible.

Our unstructured spatial discretization schemes are conservative, i.e., they preserve the kinetic energy equation, which allow good stability properties even at high Reynolds numbers and with coarse meshes. These conservation properties are held if and only if the discrete convective operator is skew-symmetric ($\mathbf{C}_c(\mathbf{u}_c) = -\mathbf{C}_c^*(\mathbf{u}_c)$), if the negative conjugate transpose of the discrete gradient operator is exactly equal to the divergence operator ($-(\Omega_c \mathbf{G}_c)^* = \mathbf{M}_c$). If the convective and gradient operators are properly chosen, the global kinetic energy equation reduces to:

$$\frac{\partial}{\partial t} \|\mathbf{u}_c\|^2 = -\mathbf{u}_c^* (\mathbf{D}_c + \mathbf{D}_c^*) \mathbf{u}_c \quad (7)$$

Since the diffusive terms must be strictly dissipative operator ($\mathbf{u}_c^* (\mathbf{D}_c + \mathbf{D}_c^*) \mathbf{u}_c \geq 0$) is symmetric and positive-definite.

To solve the velocity-pressure coupling, a classical fractional step projection method (17) is used,

$$\mathbf{u}_c^p = \mathbf{u}_c^{n+1} + \mathbf{G}_c \tilde{\mathbf{p}}_c \quad (8)$$

where the pseudo-pressure is $\tilde{\mathbf{p}}_c = \tilde{\mathbf{p}}_c^{n+1} \Delta t / (\beta + 1/2)$ and \mathbf{u}_c^p is the predicted velocity. The discrete Poisson equation for $\tilde{\mathbf{p}}_c$ is obtained by taking the divergence of equation (9) and after applying the incompressibility condition,

$$\mathbf{L}_c \tilde{\mathbf{p}}_c = \mathbf{M}_c \mathbf{u}_c^p \quad (9)$$

where the discrete Laplacian operator $\mathbf{L}_c \in \mathbb{R}^{q \times q}$ is, by construction, a symmetric positive definite matrix ($\mathbf{L}_c \equiv \mathbf{M}_c \Omega^{-1} \mathbf{M}_c^*$). Once the solution is obtained, \mathbf{u}_c^{n+1} results from the correction: $\mathbf{u}_c^{n+1} = \mathbf{u}_c^p - \mathbf{G}_c \tilde{\mathbf{p}}_c$.

2.2 Large Eddy Simulation model

We restrict ourselves to the non-equilibrium fixed-parameter SGS model from Yoshizawa (18). In the quest for a correct modelling of Navier Stokes equations, they can be filtered spatially like in Large Eddy Simulation (LES). Doing so, the filtered non-linear convective term must be modelled,

$$\rho \frac{\partial \bar{\mathbf{u}}_c}{\partial t} + \mathbf{C}(\bar{\mathbf{u}}_c) \bar{\mathbf{u}}_c + \mathbf{D} \bar{\mathbf{u}}_c + \mathbf{G} \bar{\mathbf{p}}_c = \mathbf{C}(\bar{\mathbf{u}}_c) \bar{\mathbf{u}}_c - \overline{\mathbf{C}(\mathbf{u}_c) \mathbf{u}_c} \approx - \frac{\partial \tau_{ij}}{\partial x_j} \quad (10)$$

where the filtered velocity is denoted by $\bar{\mathbf{u}}_c$ and the SGS stress (τ_{ij}) is defined as, $-2\nu_s \bar{\mathbf{S}}_{ij} + \frac{1}{3} \tau_{ij} \delta_{ij}$. Now, we only need to define a suitable expression for the SGS viscosity. Smagorinsky has proposed the following model (19),

$$\nu_s = (C_s \Delta)^2 \left(2 |\bar{\mathbf{S}}_{ij}|^2 \right)^{1/2} \quad (11)$$

Unfortunately this model is not appropriate in the close vicinity of a solid wall subject to dominant molecular-viscosity effects. To overcome these limitations Yoshizawa has derived non-equilibrium fixed-parameter SGS model,

$$\nu_s = C_{vs} \Delta \left\| \bar{\mathbf{u}}_c - \bar{\bar{\mathbf{u}}}_c \right\| \left(1 - \exp \left(- \left(C_w \left\| \bar{\mathbf{u}}_c - \bar{\bar{\mathbf{u}}}_c \right\| / \bar{\mathbf{s}} \Delta \right)^2 \right) \right) \quad (12)$$

Where $\bar{\bar{\mathbf{u}}}_c$ is the doubly filtered velocity and $\bar{\mathbf{s}} = \left(2 |\bar{\mathbf{S}}_{ij}|^2 \right)^{1/2}$. In this model the equilibrium of SGS fluctuation is not assumed, no use is made of wall-unit distance based on the friction velocity and the near-wall asymptotic behaviour of the SGS viscosity is fulfilled. None of these properties are included in the standard Smagorinsky model. In fact, in his original paper, Yoshizawa's final conclusion is that this model possesses the features similar to the dynamic SGS modelling without the classical instability of the dynamical models.

3 COMPUTATIONAL DOMAIN, MESH AND BOUNDARY CONDITIONS

The geometry of compressor valve reed has been modelled as an axial feeding plus a perpendicular diffuser followed by a discharge zone. The following geometrical values have been considered: $l_h=2l_v$; $e=d$ and $D=3d$. Figure 2 shows the whole computational domain and a half zoom of the valve seat, together with valve reed and fluid gap, respectively. The numerical results presented have been obtained with a mesh of 250000 CVs over 32 planes.

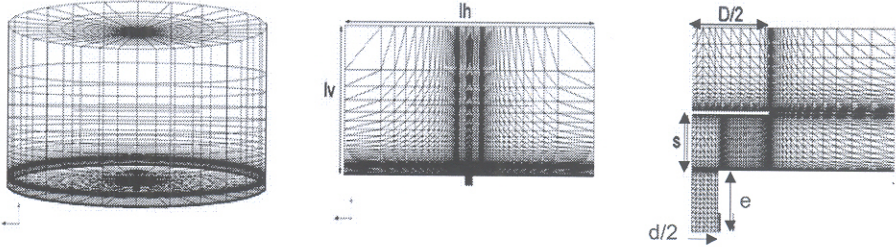


Figure 2. Valve mesh and domain. General view (left); plane section (middle) and zoom view (right).

Figure 2 depicts the whole mesh domain, two of the 32 planes on angular division and a zoom view near valve plate and valve reed. The mesh is composed by 4 horizontal zones from bottom to top: i) inlet orifice zone of 50 nodes; ii) down valve zone of 40 nodes; iii) parallel zone around the valve of 12 nodes and iv) up valve zone of 30 nodes. The same mesh domain is divided by 3 vertical zones from left to right: i) valve plate orifice under valve reed of 30 nodes and over valve reed of 5 nodes; ii) between valve plate orifice and right orifice under valve plate of 80 nodes and over valve plate of 20 nodes; and iii) right valve part of 30 nodes. In addition to this, exponential concentration mesh closer to reed valve is considered at each zone.

The boundary conditions for the simulated cases are: i) Bottom inlet orifice: constant velocity for Re numbers from 600 to 6000; ii) Bottom part and valve reed: non-slip boundary conditions on solid wall; iii) Lateral domain: Neumann boundary conditions, and iv) Top outlet fluid exit: $p_o = p_b \gamma_b (\rho_b v_b^2) / 2$. The turbulence model used is non-equilibrium fixed-parameter SGS model. For the solution of the pressure equation a Direct Fourier Schur Decomposition (20) solver is used. Twenty four hours of computation time are necessary in order to achieve the statistically stationary motion using 2 CPUs.

4 NUMERICAL RESULTS

Figure 3 depicts non-dimensional fluid pressure maps $p^* = 2\bar{p}/(\rho v_u^2)$ for Re number of 600, 3000 and 6000 from top to bottom, and gap ratios of 0.1, 0.2, 0.3, 0.6 and 0.9 form left to right.

The numerical results of Figure 3 shows that: i) pressure distribution for gap ratios lower than 0.2 is high, uniform along valve plate orifice and equal on valve reed for radius between 0 and $d/2$, while for the rest of the valve reed pressure is very low; ii) pressure distribution for gap ratios between 0.2 and 0.6 presents different gradients from inlet orifice to downer part of reed valve and different pressure profile along the downer part of valve reed for radius between 0 and $d/2$ than

radius between $d/2$ and $D/2$; and iii) for gap ratios higher than 0.6 circulating effects are added at the exit of the valve reed through the gap. The same phenomenon takes place for all studied Re numbers.

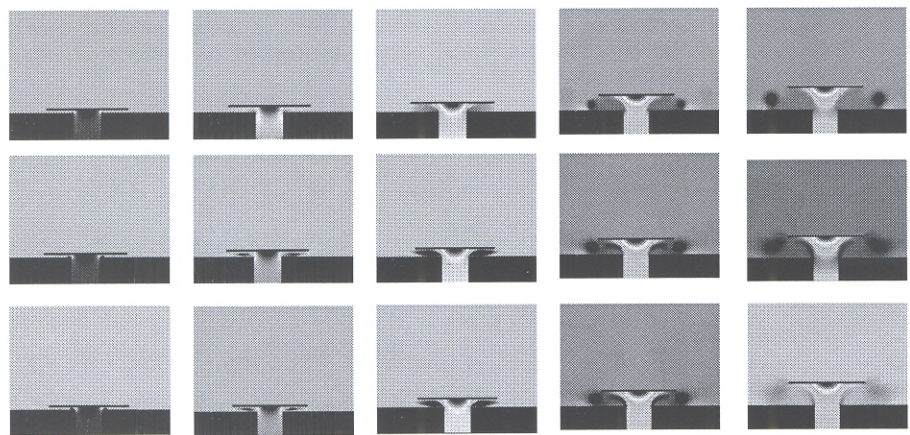


Figure 3. General view of mean pressure maps.

Figure 4 depicts non-dimensional pressure values $p^* = 2\bar{p}/(\rho v_u^2)$ for gap ratios of 0.1, 0.2, 0.3, 0.6 at the different Re numbers of 600, 3000 and 6000, respectively. The numerical values of Figure 4 are in fact the pressure profile under the valve of Figure 3.

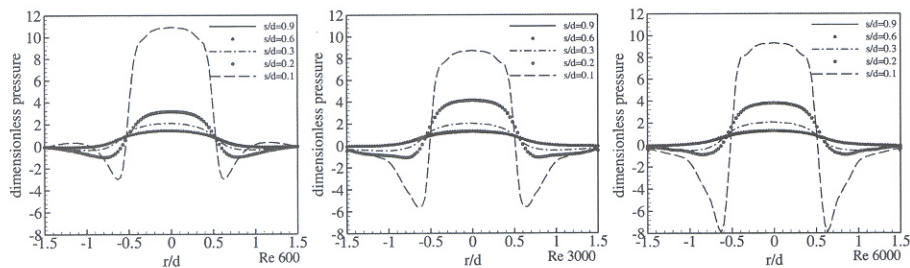


Figure 4. Numerical results of non-dimensional pressure under valve reed.

The numerical results of Figure 4 shows how under small gaps negative forces act over the reed valve closing it to the valve plate. This effect is drastically reduced for s/d ratios higher than 0.2, although it appears under all studied Re numbers.

Numerical values that allow knowing the forces caused by the turbulent radial outflow are the pressure distribution under the valve disk. In that sense the numerical results of effective force and flow area are based on Figure 4 results.

Figure 5 depicts non-dimensional fluid velocity profile $v^* = \bar{v}/v_u$ for Re number of 600, 3000 and 6000 from top to bottom, and gap ratios of 0.1, 0.2, 0.3, 0.6 and 0.9 form left to right.

The numerical results of Figure 5 shows how: i) at low Re numbers like 600, the fluid flows quasi developed across the gap through all section at low gap ratios or close to the downer reed valve at high gap ratios; ii) for higher Re numbers of 3000 or 6000, the flow presents an impact on valve reed near the corner developing circulation flows at the end of the gap and occupying all gap section at low gap ratios or flowing close to the downer reed valve at high gap ratios.

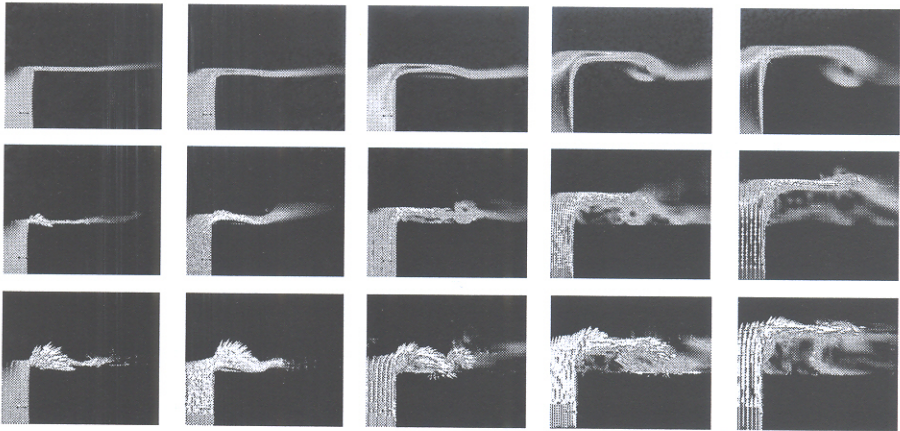


Figure 5. General view of instantaneous plane velocity field.

Based on the numerical results presented above, a global values of non-dimensional force $F^* = F / (\rho v_o^2 d^2)$, effective force $A_F^* = A_F / d^2$ and flow areas $(KA)_e^* = (KA)_e / d^2$ (1)(2) are shown in an non-dimensional way. Figure 6 shows both non-dimensional effective force and flow areas considering the Reynolds numbers of 600, 3000 and 6000, together with the s/d ratios of 0.1, 0.3, 0.6 and 0.9.

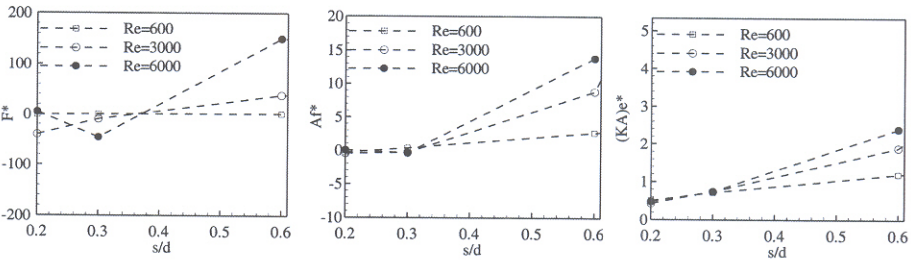


Figure 6. Numerical results of non-dimensional force and effective force and flow areas.

Although the numerical results obtained are not points enough to show the global values tendency, the points obtained presents a reasonable agreement with (4)(9) results available on research literature.

Based on the numerical results obtained for s/d ratios between 0.2 and 0.6 it is possible to conclude that: i) Effective force and flow areas increase when s/d ratio increases; and ii) Effective force and flow area presents different slopes increasing when Re number increases.

CONCLUSIONS

A numerical study of the turbulence fluid flow through valve reed has been presented based on a CFD&HT code considering 3D axial symmetric coordinates under Large Eddy Simulation turbulence models. First preliminary results are depicted in order to show pressure maps evolution and velocity maps profile with the aim to determine the forces under the valve and their non-dimensional effective force and flow area parameters.

REFERENCES

- (1) O. Lehmkuhl, R. Borrell, C.D. Pérez-Segarra, M. Soria, A. Oliva, A new parallel unstructured CFD code for the simulation of turbulent industrial problems on low cost PC cluster, *Parallel Computational Fluid Dynamics*, Ankara, Turkey, 2007.
- (2) W. Rodi, DNS and LES of some engineering flows, *Fluid Dynamic Research*, vol. 38, pp. 145-173, 2006
- (3) R. Borrell, O. Lehmkuhl, M. Soria, A. Oliva; Direct Schur method for the solution of Poisson equation with unstructured meshes; *Parallel CFD Congress*, Antalya, Turkey, 2007.
- (4) W. Soedel, Mechanics, Simulation and design of compressor valves, gas passages and pulsation mufflers, Purdue University, 1992.
- (5) C.D. Pérez-Segarra, J. Rigola, A. Oliva, Modelling and numerical simulation of the thermal and fluid dynamic behaviour of hermetic reciprocating compressors. Part I: Theoretical basis, *International Journal of Heating, Ventilating, Air-Conditioning and Refrigerating Research*, vol. 9, pp. 215-236, 2003.
- (6) D.D. Schwerzler, J.F. Hamilton, An Analytical Method for determining Effective Flow and Force Areas for Refrigeration Compressor Valving Systems, *International Compressor Engineering Conference*, pp. 30-36, 1972.
- (7) L. Böswirth, Theoretical and experimental study on flow in valve channels, Parts I and II, *International Compressor Engineering Conference*, pp. 38-53, 1982.
- (8) R.T.S. Ferreira, J.L., Driessen, Analysis of the influence of valve geometric parameters on the effective flow and force areas, *International Compressor Engineering Conference*, pp. 632-646, 1986
- (9) C.J. Deschamps, R.T.S. Ferreira, A.T. Prata, Turbulent Flow Through Valves of Reciprocating Compressors, *International Compressor Engineering Conference*, pp. 377-382, Purdue University, Indiana, 1996.
- (10) C.D. Pérez-Segarra, A., Oliva, M. Costa, F. Escanes, Numerical Experiments in Turbulent Natural and Mixed Convection in Internal Flows, *International Journal of Numerical Methods for Heat & Fluid Flow*, vol.5, No. 1, pp.13-32, 1995.
- (11) C.D. Pérez-Segarra, J., Cadafalch, J. Rigola, A. Oliva, Numerical study of turbulent fluid flow through valves, *Int. Conference on Compressors and Their Systems*, C542/021/99, 1999.
- (12) J. Rigola, O. Lehmkuhl, C.D. Pérez-Segarra, A. Oliva, Numerical simulation of fluid flow through valves based on Large Eddy Simulation models (LES), *International Compressor Engineering Conference*, 1405, Purdue University, Indiana, 2006.
- (13) C.E. Wark, J.F. Foss, Forces caused by the radial out-flow between parallel disks, *Journal of Fluids Engineering*, ASME Transactions, vol. 106, pp. 292-297, 1984.
- (14) J.S. Ervin, N.V. Suryanarayana, Hon Chai Ng, Radial, turbulent flow of a fluid between two coaxial disks, *Journal of Fluids Engineering*, ASME Transactions, vol. 106, pp. 378-383, 1989.

- (15) S Satake, T. Kunugi, Direct numerical simulation of an impinging jet into parallel disks, *Int. J. of Numerical Methods for Heat and Fluid Flow*, vol. 8, no. 7, pp. 768-780, 1998.
- (16) M. Lygren, H.I. Anderson, Turbulent flow between a rotating and a stationary disk, *Journal of Fluids Mechanics*, vol. 426, pp. 297-326, 2001.
- (17) R.W.C.P. Verstappen and A.E.P. Vedman, Symmetry-Preserving discretization of turbulent flow, *Journal of Computational Physics*, vol. 187, pp. 343-368, 2003.
- (18) A. Yoshizawa, K. Kobayashi, T. Kobayashi, N. Taniguchi, A non-equilibrium fixed parameter subgrid-scale model obeying the near wall asymptotic constraint, *Physics of Fluids*, vol. 12, no. 9, pp. 2338, 2000.
- (19) P. Sagaut. *Large Eddy Simulation for Incompressible Flows*. Springer-Verlag, 2001.
- (20) F.X. Trias, M. Soria, C.D. Pérez-Segarra, A. Oliva, A direct Schur-Fourier decomposition for the efficient solution of high-order Poisson equations on loosely coupled parallel computers, *Numerical Linear Algebra with Applications*, vol. 13, pp. 303-326, 2006.